OPTICS

Reconfigurable entanglement distribution network based on pump management of a spontaneous four-wave mixing source

Jingyuan Liu[1], Dongning Liu[1], Zhanping Jin[1], Zhihao Lin[1], Hao Li[2], Lixing You[2], Xue Feng[1], Fang Liu[1], Kaiyu Cui[1], Wei Zhang[1,3]*, Yidong Huang[1,3]*

Leveraging the unique properties of quantum entanglement, quantum entanglement distribution networks support multiple quantum information applications and are essential to the development of quantum networks. However, practical implementation poses fundamental challenges to network scalability and flexibility. Here, we propose a reconfigurable entanglement distribution network scheme based on tunable multipump excitation of a spontaneous four-wave mixing (SFWM) source and a time-sharing method. We characterize the two-photon correlation under different pump conditions to demonstrate the effect of pump degenerate and pump nondegenerate SFWM processes on the two-photon correlation and its tunability. Then, as a benchmark application, a 10-user fully connected quantum key distribution network is established in a time-sharing way with triple pump lights. Our results provide a promising networking scheme for large-scale entanglement distribution networks owing to its scalability, functionality, and reconfigurability.

INTRODUCTION

The quantum entanglement distribution network is an important stage in the development of quantum networks, which generates end-to-end quantum entanglement in a deterministic or heralded way (*1*). It enables various quantum information applications, such as quantum key distribution (QKD) (*2*–*4*), quantum teleportation (*5*, *6*), distributed quantum computing (*7*), and quantum metrology and sensing (*8*, *9*). The most intriguing thing among these applications is the potential to implement device-independent protocols (*10*, *11*). To realize entanglement distribution between multiple users, a natural method is using wavelength division multiplexing (WDM). So far, based on WDM, efforts have been made to realize entanglement distribution networks via active routing by optical switches (*12*, *13*) or passive splitting by beam splitters (BSs) (*14*). However, the network topologies of these works are simple and they suffer from problems caused by the duty cycle of optical switches or probabilistic splitting. In addition, the entanglement distribution network with trusted nodes (*15*) was proposed to increase the user number of a QKD network, while it still has potential security risks due to these nodes.

In recent years, there have been several remarkable works exploring the construction method of entanglement distribution networks. The concept of a fully connected network based on WDM is proposed and implemented with four users (*16*). In this scheme, each user pair exclusively occupies a pair of frequency channels. It is an ideal case for the entanglement distribution network because there is a one-to-one correspondence between the user link and the frequency pair of entanglement resource. However, the number of required wavelength channels is $O(N^2)$ for N users, which limits the further increase of user number because the wavelength channels are precious resources. To increase the user number of a fully connected network, passive multi-port BSs are used to probabilistically distribute an entanglement resource to multiple user pairs (*17*, *18*). This strategy is rather suitable for large-scale QKD networks with postprocessing, while it may cause problems in other applications, such as teleporting a quantum state. Recently, some works introduced wavelength selective switch (WSS) (*19*–*21*) technology and the concept of a quantum reconfigurable optical add-drop multiplexer (q-ROADM) (*22*, *23*), which consists of filters, optical fiber switches, and WSS, to the entanglement distribution network to dynamically reconfigure the network. Nevertheless, they also suffer from the problems of either limited user numbers or probabilistic entanglement distribution. Therefore, it is necessary to propose a networking scheme for entanglement distribution networks that can tackle these two problems simultaneously.

Here, we present a reconfigurable entanglement distribution network architecture by using multiple tunable lasers to pump the spontaneous four-wave mixing (SFWM) process in a silicon waveguide chip, combined with a time-sharing method. We define this scheme as a pump management scheme, where the network topology is switched by tuning the pump frequencies and the physical structure of the network is unchanged. We first characterize the generated energy-time entangled photon pairs under different pump conditions. The quantum correlation between different frequency pairs shows a complex feature determined by the SFWM processes with degenerate and nondegenerate pump photons. The tunability of the two-photon correlation is demonstrated by changing the pump frequencies, and the two-photon energy-time entanglement is verified by Franson-type interference. Further, we demonstrate a 10-user fully connected entanglement distribution network via pump management, and a QKD network is established as a benchmark application. The number of required wavelength channels is relaxed to $O(N)$ for N users, rather than the quadratic relation in the WDM-based network. At the same time, there is no probabilistic beam splitting

[1]Department of Electronic Engineering, Tsinghua University, Frontier Science Center for Quantum Information, Beijing National Research Center for Information Science and Technology (BNRist), Beijing 100084, China. [2]National Key Laboratory of Materials for Integrated Circuits, Shanghai Institute of Microsystem and Information Technology, Chinese Academy of Sciences, Shanghai 200050, China. [3]Beijing Academy of Quantum Information Sciences, Beijing 100193, China.
*Corresponding author. Email: zwei@tsinghua.edu.cn (W.Z.); yidonghuang@tsinghua.edu.cn (Y.H.)

used in the network so that each user pair exclusively occupies a frequency pair of entanglement resources, showing potential for full-fledged quantum networks in the future.

RESULTS

Pump management for SFWM

For $\chi^{(3)}$ nonlinear materials, SFWM enables the generation of energy-time entangled photon pairs when energy conservation and phase matching conditions are satisfied (*24*). The near-zero dispersion of the $\chi^{(3)}$ nonlinear materials, such as properly designed optical fibers and silicon wire waveguides, leads to the broadband characteristic of the entangled photon pairs. It also allows the frequency of the pump light to vary over a wide frequency range, adding an additional control parameter to manipulate the SFWM process. On the other hand, according to whether the two pump photons in an SFWM process have the same frequency, the SFWM processes are classified into two cases with degenerate pump photons $\omega_{p1} = \omega_{p2}$ and nondegenerate pump photons $\omega_{p1} \neq \omega_{p2}$ (*25*–*29*), as shown in Fig. 1A. Compared with $\chi^{(2)}$ nonlinear processes, different energy conservation conditions of the SFWM processes provide the possibility to manipulate the spectral correlations between generated photon pairs by controlling the pump lights. For simplicity, the following discussion about degenerate and nondegenerate SFWM refers to the discussion about pump photons.

Here, we define the pump management scheme as flexibly changing the number and frequency of pump lasers to realize a network with the desired topology. Through the management of SFWM pump lights, it is easy to realize a fully connected entanglement distribution network in which each user receives photons in a single frequency channel. On one hand, in the case of multiple pump lights, several SFWM processes occur simultaneously, resulting in a complex two-photon correlation feature between photons with different frequencies. For instance, when two lasers with frequencies ω_1 and ω_2 pump the $\chi^{(3)}$ nonlinear material, the frequencies of SFWM pump photons $\omega_{p1}, \omega_{p2} \in \{\omega_1, \omega_2\}$ and both degenerate and nondegenerate SFWM processes will occur. The pumping scheme with dual pumps is shown in Fig. 1B. The degenerate SFWM generates signal and idler photons with pairwise correlations that are symmetric about each pump frequency, shown by solid up arrows. For the nondegenerate SFWM processes, the generated pairwise correlations are symmetric about the mean value of the two pump frequencies, shown by dashed up arrows. In this case, if we select photons at the specific four frequencies $\omega_A, \omega_B, \omega_C$, and ω_D with the relation of $|\omega_A - \omega_1| = |\omega_B - \omega_1| = |\omega_C - \omega_2| = |\omega_D - \omega_2|$, and distribute them to four users respectively, a four-user entanglement distribution network with ring-type topology is established.

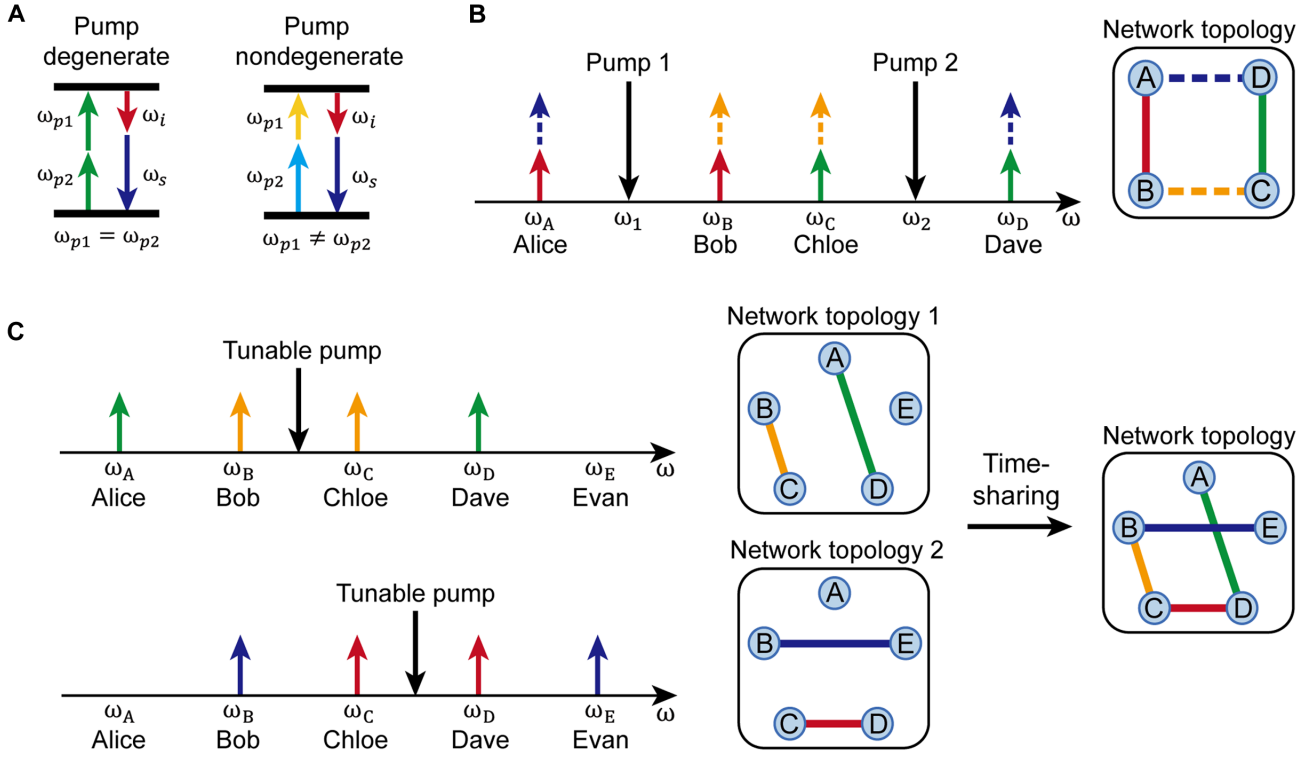

Fig. 1. Schematics of entanglement distribution network using SFWM pump management. (**A**) Diagram of energy conservation relations for SFWM processes with degenerate and nondegenerate pump photons. (**B**) The pumping scheme of a ring-type quantum network via dual pumps. Two lasers with different frequencies are used to pump the $\chi^{(3)}$ nonlinear material. Solid and dashed up arrows represent photons generated by degenerate and nondegenerate SFWM processes, respectively. Here, a pair of entangled photons are shown in the same color. By using filters to select photons of different frequency channels and distribute them to different users respectively, an entanglement distribution network with a specific topology is established. (**C**) The realization of a reconfigurable entanglement distribution network with a tunable pump. The frequency of the pump light is changed to realize different network topologies. Then, the network is established in a time-sharing way with more topological links.

On the other hand, the network topology can be dynamically reconfigured by changing the frequency of pump lights. Using a time-sharing method, network topologies complement each other to form a network with more topological links, as shown in Fig. 1C. The overall coincidence count rate is the total number of coincidence count events divided by the total time. The time-shared network reduces the number of user links that are connected simultaneously. Under some specific conditions, such as in systems with a high timing jitter of detector or low heralding efficiency of the entanglement source, it outperforms the network with all links connected at the same time (*22*, *23*). It is worth noting that each network user only receives photons in a single frequency channel, while the frequencies of pump lights change at different times. Therefore, the experimental setup will be quite simple compared with the WDM-based quantum networks.

Experimental setup

To demonstrate the effect of pump management on the generation of entangled photon pairs, we first characterize the two-photon correlation under different pump conditions. Figure 2A illustrates the experimental setup to measure two-photon joint spectral intensity (JSI). Three continuous-wave (CW) pump lasers with tunable frequencies are multiplexed through standard dense wavelength division multiplexing (DWDM) filters. Then, the light excites the SFWM process in a 10-mm-long silicon waveguide. At the output, the pump light is rejected using DWDM filters. A programmable filter (Finisar Waveshaper) selects signal and idler photons with tunable frequencies and sends them to the superconducting nanowire single-photon detectors (SNSPDs). For the correlation measurement between nondegenerate signal and idler photons, two output ports of the Waveshaper are used. In the case of degenerate photons, only one output port of the Waveshaper is used, and a BS further divides the photons into two parts before being detected by SNSPDs. Subsequently, the two-photon JSI is measured by time-resolved coincidence measurement of signal and idler photons with different frequencies.

By using the pump management strategy, we implement a 10-user fully connected entanglement-based QKD network, in which each user receives photons with a single frequency channel. The illustration of the QKD network experimental setup is schematically depicted in Fig. 2B. The generated photons from the quantum light source are separated by an arrayed waveguide grating (AWG) system according to the 100-GHz International Telecommunication Union (ITU) channels. The noise photons outside the filter band are further suppressed using DWDM filters. Then, each user receives

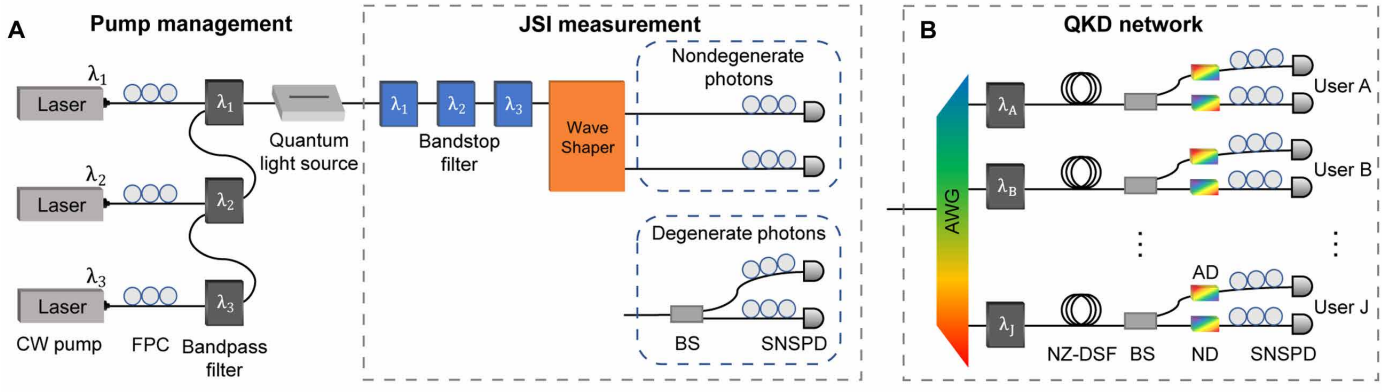

C

Wavelength allocation

User	A	B	C	D	E
ITU Ch.	C22	C26	C30	C34	C38
User	**F**	**G**	**H**	**I**	**J**
ITU Ch.	C42	C46	C50	C54	C58

D

Pump configuration

Case	Pump 1	Pump 2	Pump 3
1	C20	C40	C60
2	C24	C28	C48
3	C28	C40	C52
4	C32	C52	C56

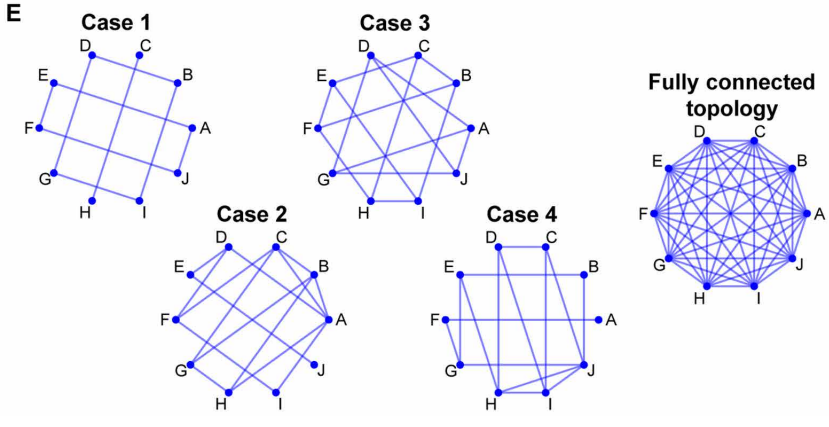

Fig. 2. Schematics of the experimental setup. (**A**) The setup for two-photon JSI measurement. The tunable pump lights are multiplexed using standard DWDM filters and coupled into a silicon waveguide chip to generate entangled photon pairs through SFWM. At the output, filters are used to reject the pump laser and select signal and idler photons with tunable frequencies. FPC, fiber polarization controller. (**B**) The setup for the 10-user QKD network after the quantum light source. The photons generated from the quantum light source are demultiplexed using AWG and DWDM filters. Each user receives photons in a single frequency channel. A BS and dispersion modules with anomalous and normal dispersion are used to construct two detection bases of symmetric dispersive optics quantum key distribution (DO-QKD). AD, anomalous dispersion; ND, normal dispersion. (**C**) Wavelength allocation scheme and (**D**) pump configuration for the 10-user fully connected entanglement distribution network. (**E**) Network topologies under four pump configurations and the generated fully connected network topology using time-sharing.

only one specific wavelength channel via a 6.2-km nonzero dispersion shifted fiber spool. Therefore, the effective separation between every two users is 12.4 km.

For each user, a 50:50 BS is used to randomly choose between the two detection bases. Then, a symmetric dispersive optics QKD (DO-QKD) configuration (*15*) is constructed by placing the dispersion modules with normal and anomalous dispersion (±1981 ps/nm at 1545 nm) at two paths on each user's side. For a two-user QKD process, the two detection bases are defined as the cases where one user detects with normal dispersion and the other user detects with anomalous dispersion, and vice versa. Nonlocal dispersion cancellation (*30*) happens in each detection basis, which is the basis of security analysis (*31*–*33*). The compensation for transmission dispersion is not performed because it is unnecessary in DO-QKD with a short transmission distance (see the Supplementary Materials). The symmetric DO-QKD has been proven to be equivalent to the conventional DO-QKD scheme (*31*), while it is more suitable for entanglement-based QKD networks because every end user has the same receiver configuration. Another important feature of DO-QKD is that it encodes the arrival times of photons in a high-dimensional way to use single-photon events more efficiently (see Materials and Methods and the Supplementary Materials).

Network architecture

Unlike the WDM-based entanglement distribution network, whose topology is based on the distribution of frequency pairs, the topology of the network with pump management depends mostly on the pump scheme, rather than the physical experimental setup. In the process of designing the wavelength allocation and pump configuration schemes, three principles are mainly considered. First, in each pump configuration, the frequencies of pump lights and the users are separated by at least one ITU channel, to reduce the impact of residual pump photons on the performance. Second, the number of pump configurations to be switched is minimized to maximize the key rate in a time-sharing scheme. Third, the accumulated network topology is consistent with the desired topology, such as the fully connected network in our scheme.

For a 10-user fully connected QKD network, the users' wavelength allocation scheme is shown in Fig. 2C. The 10 wavelength channels are evenly distributed in the telecom C-band. The pump frequencies are properly selected among the C-band ITU channels to avoid being adjacent to the users' frequencies. If a pump frequency is the same as a user's frequency, this user will discard all photons in this situation. On the basis of the above principles, we design a 10-user fully connected network with three pump excitations. The three pump lights switch between four configurations, as shown in Fig. 2D. In each case, a QKD network is temporarily established with the designed topology shown in Fig. 2E. The lines between different user nodes represent the quantum correlation of entangled photon pairs. Using the time-sharing method, a fully connected network is established based on the results under the four pump configurations.

Characterization of two-photon correlation under different pump conditions

To measure the two-photon correlation, we first pump the quantum light source using a single laser with a tunable frequency. The pumping scheme is depicted in Fig. 3A with the pump power before coupling into the chip of about 2 mW. For the JSI measurements here, the Waveshaper routes signal and idler photons whose central frequencies correspond to those of the 100-GHz ITU grid channels; however, the bandwidth is set to be 25 GHz to prevent a high single-photon count rate from saturating the SNSPDs. In the single pump situations, the degenerate SFWM occurs in the quantum light source, generating photon pairs with pairwise correlation that are symmetric about the pump frequency, as schematically depicted in Fig. 3B. We tune the pump frequency to correspond to 100-GHz ITU channels of C30, C40, and C50, and the obtained JSI results are shown in Fig. 3 (C to E, respectively). It reveals the strong frequency anticorrelation determined by the energy conservation conditions and the tunability of the two-photon correlation. Under different pump frequencies, the coincidence line shifts parallel to the diagonal because the sum of the signal and idler frequencies varies with the pump frequency. The central point of the coincidence line is excluded from the test because it involves photons of the same frequency as the pump light. The corresponding coincidence–to–accidental ratios (CARs) for each frequency pair in three pump cases are given in Fig. 3 (F to H). When approaching the pump frequency, the CAR decreases due to the influence of residual pump photons. For frequency pairs away from the pump frequency, the CAR is on the order of 1×10^3.

Adding another pump laser to the system, a more complex two-photon correlation feature will emerge. The pumping scheme is shown in Fig. 4A, and each pump power before coupling into the chip is about 2 mW. The degenerate SFWM process associated with each pump and the nondegenerate SFWM process associated with two pumps occur simultaneously, leading to a complex quantum correlation structure (see Fig. 4B). It can be divided into two sets of frequency channels with quantum correlations that can be viewed as two two-dimensional (2D) square lattice configurations. Tuning the pump frequencies of the two pump lights, the obtained JSI results are shown in Fig. 4 (C to E). Three coincidence lines emerge, with the middle line corresponding to the nondegenerate case and the other lines corresponding to the degenerate cases. It can be seen that the number of coincidence counts in the nondegenerate case is about four times higher than that in the degenerate cases, because the SFWM with distinct pump photons are more efficient in generating photon pairs than the degenerate SFWM when two pumps are launched with equal powers (*24*). As the frequency difference of the pump lights increases, the gap between the three coincidence lines also increases, which is determined by energy conservation. Furthermore, in the dual pump configuration, it is found that strong lights are generated at specific frequencies. Assuming that the pump frequencies are denoted by ω_1 and ω_2, the strong lights are generated at $2\omega_1 - \omega_2$ and $2\omega_2 - \omega_1$ due to the stimulated four-wave mixing (FWM) process (*34*) where each pump laser can also be regarded as an input signal beam. Hence, the photons at these frequencies as well as those at the pump frequencies are excluded in the test. The corresponding CAR results for each frequency pair are given in Fig. 4 (F to H). Similarly, the CAR in the nondegenerate case is also about four times higher than that in the degenerate cases. The reason is that under a fixed pump condition, the single-side count rate of each user is at the same order of magnitude, leading to similar accidental coincidence rates for all user links. Then, the difference in CAR is primarily attributed to the difference in the coincidence count rate.

Furthermore, the triple pump configuration enables more SFWM processes to occur simultaneously. The pumping scheme is shown in

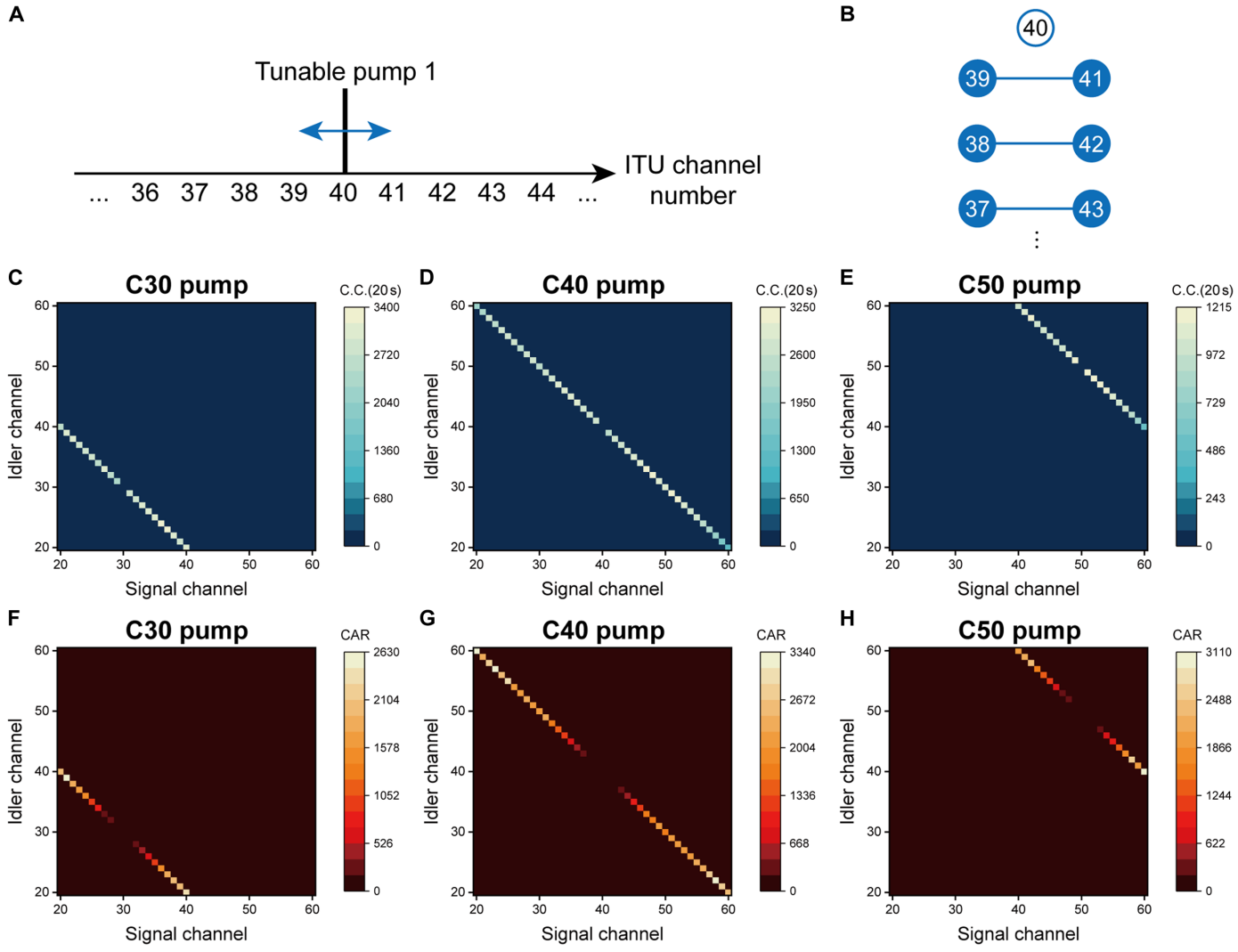

Fig. 3. Characterization of two-photon correlation in the case of a single pump. Schematic diagrams of (**A**) the pumping scheme using a tunable pump and (**B**) the generated quantum correlation between photons with different frequencies. The numbers correspond to the 100-GHz ITU channels. Assume that the pump frequency channel is C40, shown in an open circle, the signal and idler channels are symmetric about the pump channel, shown in filled circles. Then, the solid lines connecting the channels represent quantum correlations between entangled photons. (**C** to **E**) The measured two-photon JSI under different pump frequencies. There is a coincidence line parallel to the diagonal in each pump condition, which shows the spectral anticorrelation determined by energy conservation. The photons at the pump frequency are excluded from the test. The coincidence window is 200 ps in the JSI measurements of this work. The integration time for each coincidence measurement is 20 s. C.C., coincidence counts. (**F** to **H**) The CAR results under different pump frequencies.

Fig. 5A, and each pump power before coupling into the chip is about 2 mW as well. In this case, the degenerate SFWM process associated with each pump and the nondegenerate SFWM process associated with every two pumps occur simultaneously. The structure of the generated quantum correlation is more complex, which can be divided into two sets of 3D cubic lattices with different frequency channels (see Fig. 5B). There are six types of SFWM energy conservation relations based on the three pump frequencies. Therefore, the number of coincidence lines in the two-photon JSI is five or six (see Fig. 5, C to F) depending on whether the pumps are equispaced in frequency or not. To avoid saturation of SNSPDs, there is an additional loss introduced by variable optical attenuators before the detection of 3.7, 7.5, 4.6, and 0 dB for Fig. 5 (C to F, respectively). In addition to the phenomena discussed in the two configurations above, strong lights are generated at more specific frequencies in the triple pump configuration. Assuming that the pump frequencies are denoted by ω_1, ω_2, and ω_3, the strong lights are generated at $2\omega_1 - \omega_2$, $2\omega_1 - \omega_3$, $2\omega_2 - \omega_1$, $2\omega_2 - \omega_3$, $2\omega_3 - \omega_1$, and $2\omega_3 - \omega_2$ due to the stimulated FWM process. Given that FWM Bragg scattering involves two pump fields and a signal field (*35*), in the triple pump configuration, the strong lights are also generated at $\omega_1 + \omega_2 - \omega_3$, $\omega_1 - \omega_2 + \omega_3$, and $-\omega_1 + \omega_2 + \omega_3$. Similarly, the photons at these frequencies as well as the pump frequencies are discarded. The corresponding CAR results for each frequency pair are given in Fig. 5 (G to J). The situations with equispaced pumps outperform the situation with nonequispaced pumps in terms of CAR, because the number of frequencies that generate strong light is higher in the latter case. As a result, the requirement for filtering will be higher.

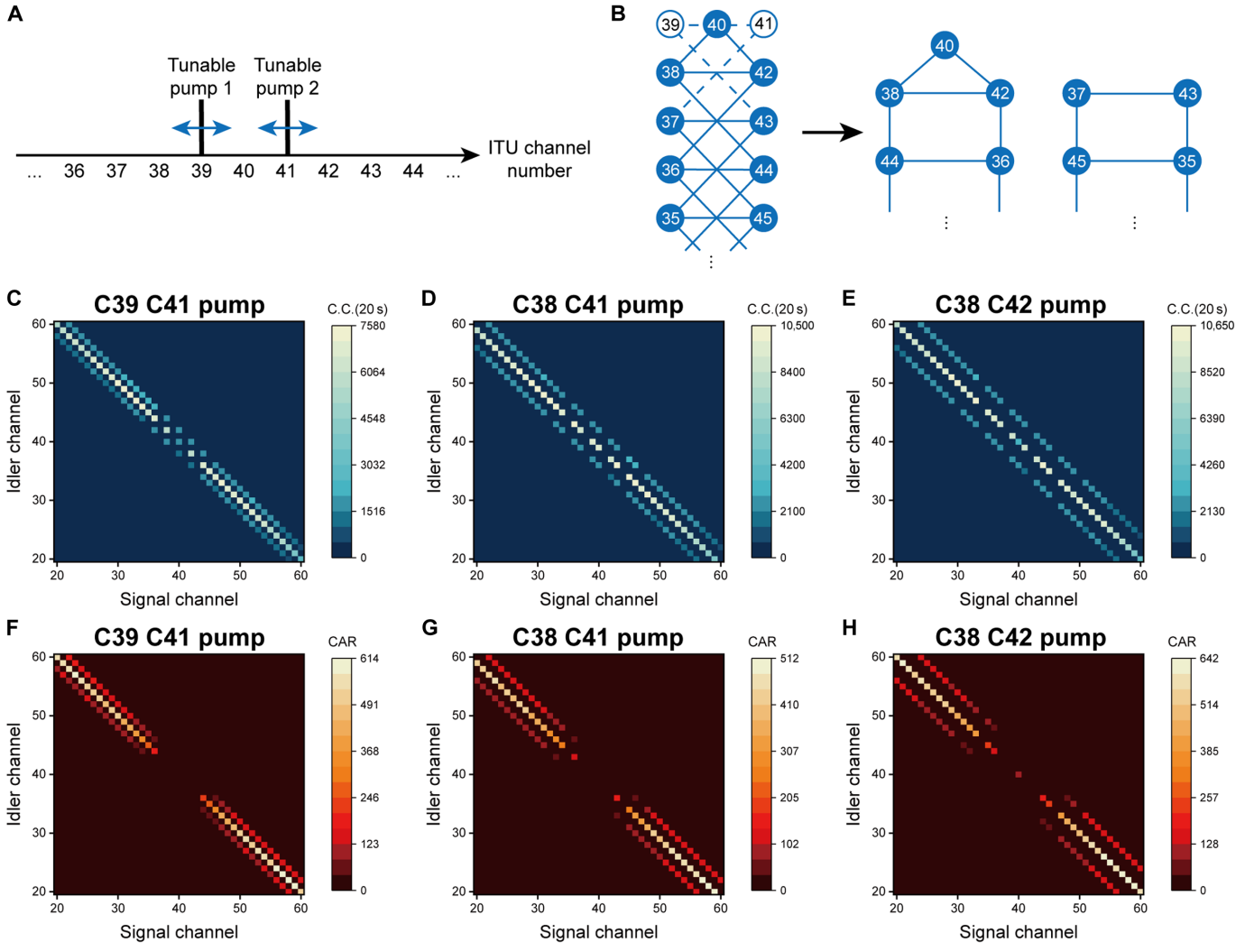

Fig. 4. Characterization of two-photon correlation in the case of dual pumps. Schematic diagrams of (**A**) the pumping scheme using two tunable pumps and (**B**) the generated quantum correlation between photons with different frequencies. The pump frequencies are assumed to be C39 and C41 for example. The dashed lines represent quantum correlations with undetected photons in our test due to pump lights and stimulated FWM. It can be divided into two sets of frequency channels with quantum correlations of 2D square lattice configurations. (**C** to **E**) The measured two-photon JSI under different pump frequencies. There are three coincidence lines parallel to the diagonal in each pump condition, which shows the spectral anticorrelation determined by energy conservation of degenerate and nondegenerate SFWM processes. The photons at the same frequencies as the generated strong light and the pump lights are excluded from the test. The integration time for each coincidence measurement is 20 s. (**F** to **H**) The CAR results under different pump frequencies.

Franson-type interference

In addition to the two-photon correlation, we characterize the energy-time entanglement of some specific frequency pairs by Franson-type interference (*36*). Under a single pump with frequency C40, Franson-type interference is implemented with each frequency pair symmetric to the pump frequency. A typical interference result is given in Fig. 6A with signal and idler photons of frequencies C37 and C43. The raw visibilities are 96.8 ± 0.5% and 96.5 ± 2.1% of the two fringes. As can be expected from the fringes of the Franon-type interference, the correlation function in the process of calculating the S parameter has a sinusoidal form. Therefore, the maximum value of the S parameter is $2\sqrt{2}V$ (V is the visibility of interference fringes) and is calculated to be 2.73 ± 0.06, with a violation of the Clauser-Horne-Shimony-Holt (CHSH) Bell inequality $S_{\max} = 2\sqrt{2}V \leq 2$ by 12 deviations (*37*, *38*). After subtracting the accidental coincidence counts, the corresponding net visibilities are 97.5 ± 0.4% and 97.4 ± 1.9%. The maximum value of the S parameter is 2.75 ± 0.05 with a violation of the CHSH Bell inequality by 15 deviations. The raw visibilities for different frequency pairs under a single pump with frequency C40 are given in Fig. 6B. For the frequency pair adjacent to the pump frequency, that is, the C39 and C41, the visibility is relatively low due to the influence of residual pump photons and Raman noise photons. Except in this case, the raw visibilities are almost above 95%, showing that high-quality energy-time entanglement is generated in a wide band.

For other pump cases, we randomly select one specific frequency pair for each SFWM process to perform Franson-type interference. For the conditions of dual pumps, three frequency pairs are selected

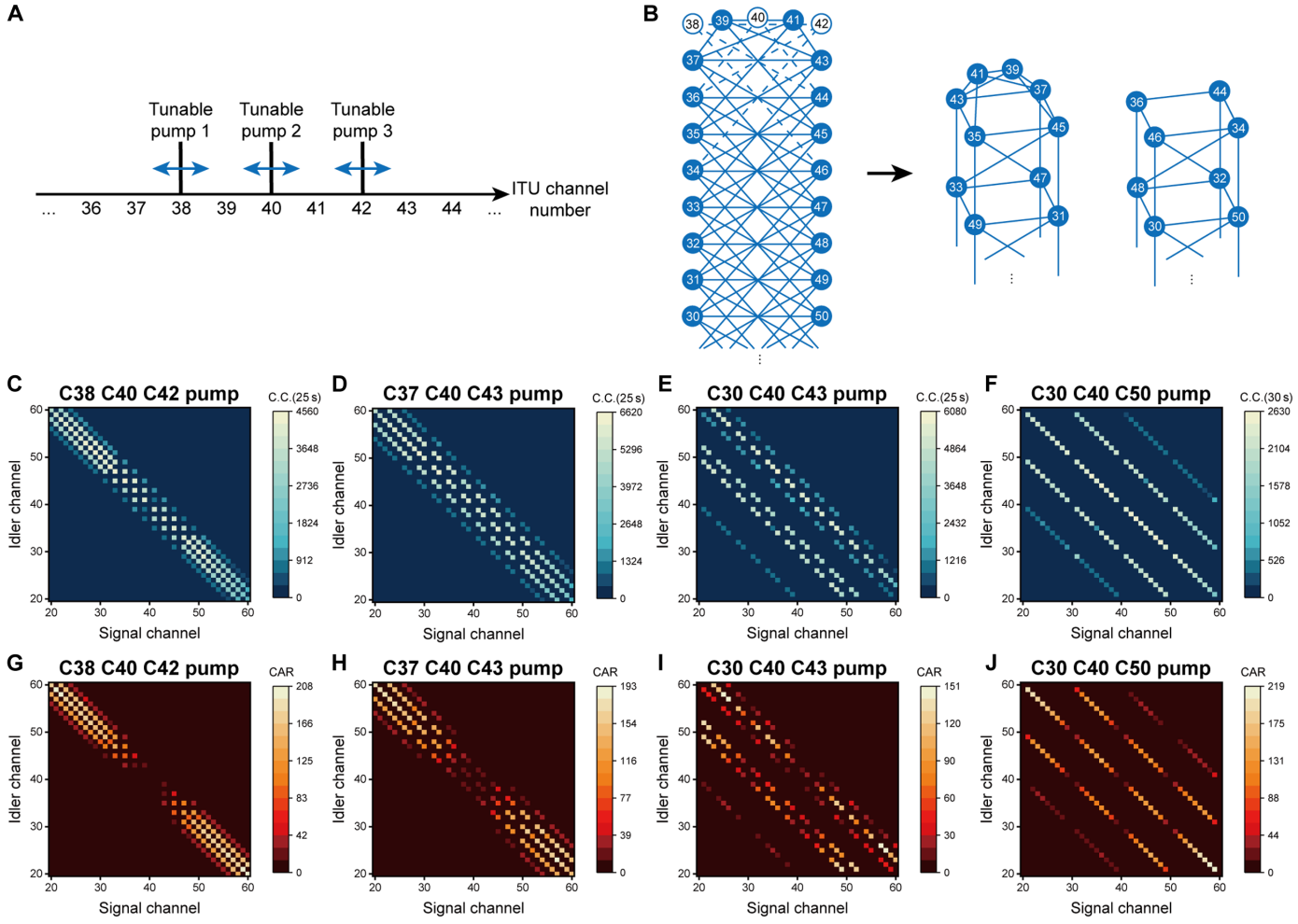

Fig. 5. Characterization of two-photon correlation in the case of triple pumps. Schematic diagrams of (**A**) the pumping scheme using three tunable pumps and (**B**) the generated quantum correlation between photons with different frequencies. The pump frequencies are assumed to be C38, C40, and C42 for example. It can be divided into two sets of 3D cubic lattices. (**C** to **F**) The measured two-photon JSI under different pump frequencies. There are five (six) coincidence lines parallel to the diagonal when ω_1 and ω_3 are symmetric (asymmetric) about ω_2. The photons at the same frequencies as the generated strong light and the pump lights are excluded from the test. The integration time for each coincidence measurement is 25 or 30 s. (**G** to **J**) The CAR results under different pump frequencies.

for each pump case. Typical visibility results under dual pumps with frequencies C39 and C41 are given in Fig. 6C. The blue bars represent the interference results of degenerate SFWM processes while the orange bar represents that of the nondegenerate SFWM process. It can be seen that the raw visibilities in the degenerate SFWM processes are lower than that in the nondegenerate SFWM process, which is mainly due to the lower CAR. However, after subtracting the accidental coincidence count, the net visibilities of the three processes are almost the same (see the Supplementary Materials for more details and results).

For the conditions of triple pumps, five or six frequency pairs are selected for each pump case, depending on whether the pumps are equispaced in frequency or not. Typical visibility results under triple pumps with frequencies C38, C40 and C42 are given in Fig. 6D. The green bar represents the interference result of a degenerate process and a nondegenerate process that produce photons of the same frequency (see fig. S7 for illustration). Because this case has the highest CAR, it has the highest raw visibility among the three conditions.

Fully connected QKD network

Subsequently, a 10-user fully connected QKD network is realized using the setup shown in Fig. 2B. With a limited number of available SNSPDs, we measure the QKD results in a pairwise way; that is, we select two users to measure at the same time while the network is established under each pump configuration. The user pairs that do not receive entangled photon pairs are unable to establish QKD; thus, these links are not measured. In each detection basis, 70% of the coincidence counts are used for key generation and the rest are used for security analysis. The high-dimensional encoding parameters are optimized for each two-user case to maximize the secure key rate (SKR) (see details in Materials and Methods) (*39*).

The pump lights are switched between four configurations to effectively reconfigure the network topology. The measurement time is 10 min for each user link to generate secure keys in the asymptotic regime. The asymptotic SKR values in four pump configurations are shown in Fig. 7 (A to D, respectively). The resulting network topologies (see insets) follow the prior designs. There is a difference

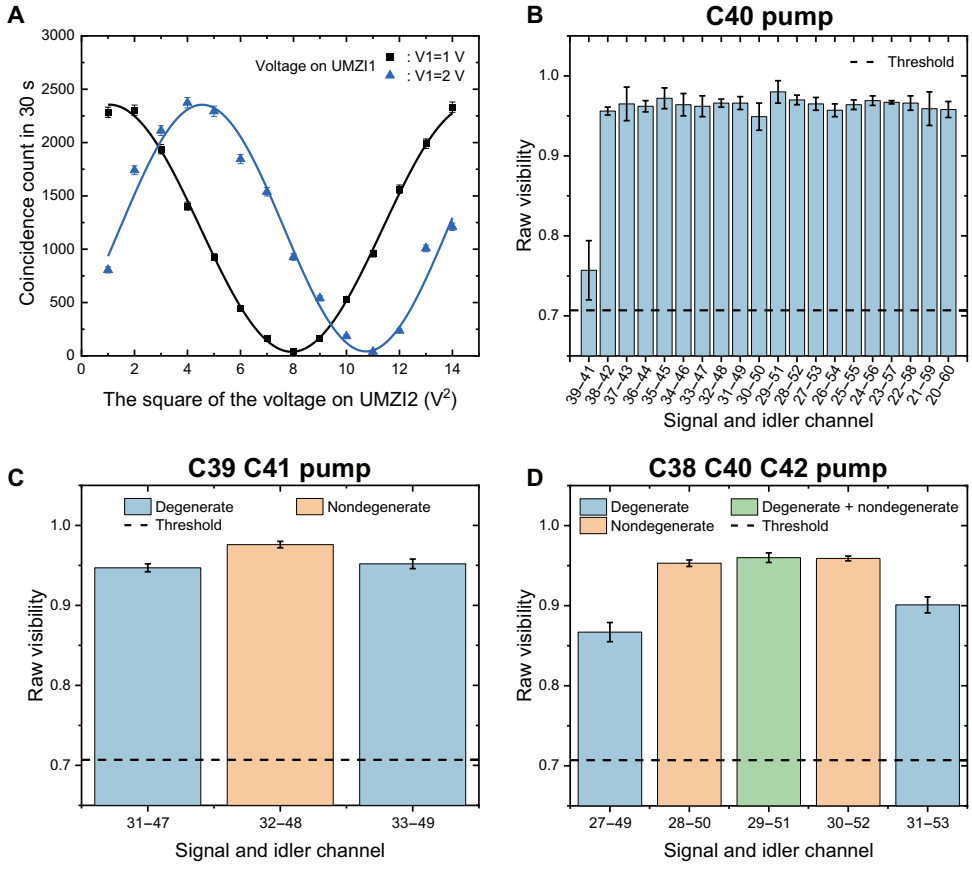

Fig. 6. Franson-type interference results. (**A**) A typical interference result under a single pump with frequency C40 without subtracting the accidental coincidence counts. The frequencies of signal and idler photons are C37 and C43. The error bars are obtained by Poissonian photon-counting statistics. The solid lines are sinusoidal fitting curves of the experimental data. (**B**) Raw visibilities of different frequency pairs under a single pump with frequency C40. The visibility of each frequency pair is chosen as the lower one of the results under two bases. (**C**) Raw visibilities under dual pumps with frequencies C39 and C41. (**D**) Raw visibilities under triple pumps with frequencies C38, C40, and C42.

in the SKRs between different user pairs, which is mainly attributed to two factors. First of all, as mentioned above, the coincidence count rate in the nondegenerate SFWM cases is about four times higher than that in the degenerate cases. Second, under a fixed pump condition, the CAR of different SFWM processes has the same relation as the coincidence count rate. It causes the DO-QKD encoding dimension to differ between user pairs after parameter optimization. Therefore, the key rate, which is proportional to the product of the coincidence count rate and the encoding dimension, is higher for links using nondegenerate SFWM than those using degenerate SFWM. After time-sharing, the overall SKR is the total number of keys divided by the total time, as shown in Fig. 7E. It can be seen that every user link above the diagonal has a positive SKR with an average value of 122.2 bps, realizing a 10-user fully connected QKD network. Considering the finite-size effect, we also successfully generate secure keys for all the user links; however, a longer measurement time is needed for some user links (see details in the Supplementary Materials).

DISCUSSION

We have demonstrated a reconfigurable entanglement distribution network scheme through pump management of an SFWM quantum light source and presented a 10-user fully connected QKD network using time-sharing. The situations of a single pump, dual pumps, and triple pumps are investigated to show the tunability of the two-photon correlation generated by SFWM. There is a difference in the SKRs between user pairs, which is mainly due to the intrinsic nature of degenerate and nondegenerate SFWM processes. Fortunately, the tunability of pump frequencies brings the possibility to optimize the network performance with a preferred outcome by prior designing the pump configurations. Additional pump configurations can be introduced to compensate for the SKR difference. However, it may be at the cost of a decrease in the average SKR.

One of the advantages of our network scheme is that the frequency utilization is higher. It uses N frequency channels to support an N-user fully connected network. Compared with the $O(N^2)$ scaling of frequency channels in WDM-based fully connected networks, the proposed scheme greatly relaxes the requirement for the number of frequency channels; thus, it can be extended to more users. Using the ITU 100-GHz grid channels, our network scheme is expected to support up to 40 users with a series of designed pump configurations and excellent pump filtering. Even a larger-scale network with more than 100 users is possible by using a finer frequency grid, e.g., the 50-GHz grid, or including the L-band frequencies.

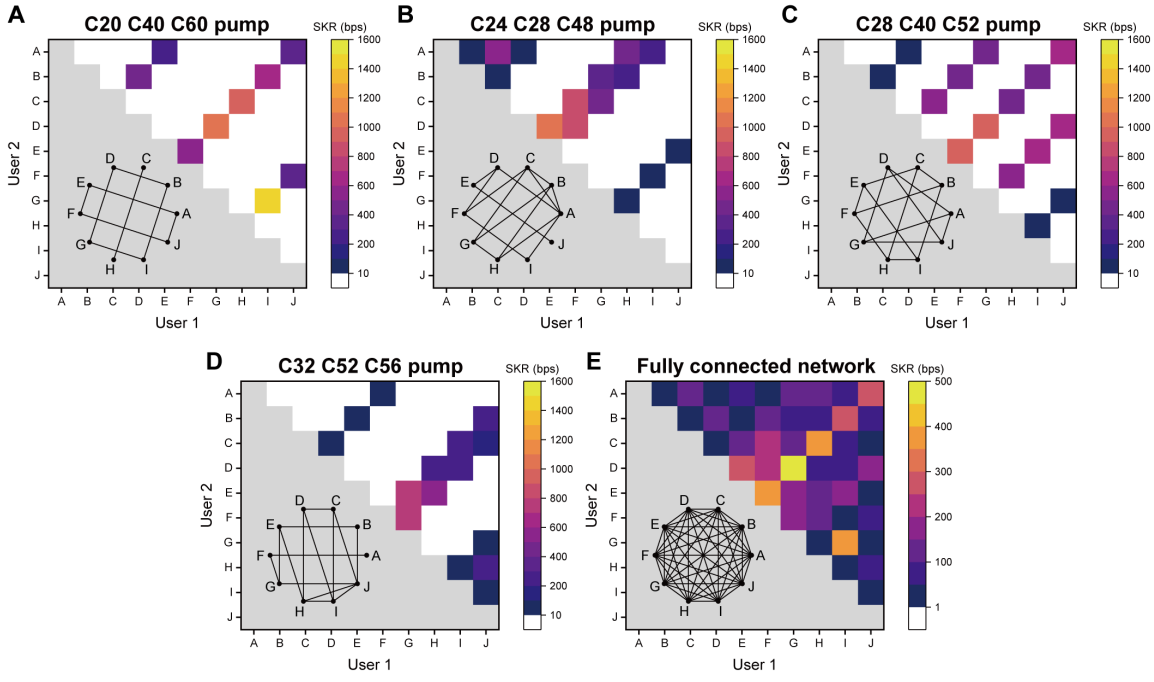

Fig. 7. Asymptotic SKR of the time-shared QKD network. (**A** to **D**) Temporary asymptotic SKR results under four pump configurations. Insets show the corresponding network topologies. (**E**) The overall asymptotic SKR result of the fully connected network using time-sharing.

In addition, another key feature of the proposed network is that each user link exclusively occupies a frequency pair of entanglement resource. There is no passive splitting in the distribution process of photons. On one side, the loss caused by the BS is avoided. On the other side, it is possible to conduct multiple quantum information applications beyond QKD. In our experiment using multiple pumps, a user may be connected to more than one user, so it can still only support applications with postprocessing, such as QKD. To distinguish each user pair, a single tunable pump is required to establish an entanglement distribution network where each user is connected to only one user. Hence, it can support quantum information applications without postprocessing at the cost of using more pump configurations.

Furthermore, the pump management scheme offers reconfigurability to the entanglement distribution networks. The frequency and power of each pump can be easily tuned to reconfigure the logical topology of the network without changing the physical links. Compared with the reconfigurable network schemes using WSS (*19*–*21*) or q-ROADM (*22*, *23*), the losses introduced by the optical switches and wavelength switches on the entangled photon pairs are avoided. In addition, our scheme is not limited to the number of output ports of WSS or q-ROADM and has higher scalability. The system loss is independent of the user number as well. We note that the network with pump management has limited reconfigurability and is unable to realize arbitrary topology at a time, so it is suitable for use with the time-sharing method.

The pump situation is not limited to triple pumps. Using more pump lights, even an optical frequency comb, to excite SFWM processes in the quantum light source may result in a more complex two-photon correlation feature. One possible challenge is that strong lights are generated at more specific frequencies, which will influence the performance of quantum information applications to a large extent. In our demonstration, the single photons at these frequencies are discarded. However, the utilization of single photons at these frequency channels decreases in this situation. Second, it also poses challenges to the filtering systems of the pump lights and the entangled photons. Third, more SFWM processes occur with an increasing number of pump lights. Then, for a specific user link, photons generated from other SFWM processes become background noise. When the number of pump lights increases, the efficient suppression of background noise is critical. We carry out theoretical analysis and numerical simulation to show how the noise photons affect the performance of Franson-type interference and QKD (see section S5). Besides, if multiple lasers coherently pump the quantum light source, quantum optical frequency combs with different spectral correlation features can be generated, adding an extra degree of freedom for quantum information processing in the frequency domain (*40*–*42*). The photons discussed above are in a bipartite entanglement state. When entangling multiple photon pairs, multiphoton entanglement would be generated with a high-dimensional lattice in the frequency domain, which would have great potential as a universal resource for measurement-based quantum computing (*43*).

In summary, we have proposed a reconfigurable entanglement distribution network scheme based on pump management and a time-sharing method. Single, dual, and triple pump lasers are used to excite the SFWM process in a silicon waveguide chip. When multiple pump lights excite the $\chi^{(3)}$ nonlinear material, SFWM processes with degenerate and nondegenerate pump photons occur simultaneously, forming complex two-photon correlation features that are characterized by JSI measurements. The energy-time entanglement of specific frequency pairs is verified by Franson-type interference. Further, we have realized a 10-user fully connected QKD network under triple pumps as a benchmark application. The quantum light source for the network is pumped under four pump configurations and the network is constructed in a time-sharing way. Our results

show the scalability, functionality, and reconfigurability of the proposed entanglement distribution network, which provides a potential architecture for future quantum networks.

MATERIALS AND METHODS

Franson-type interference experimental setup

The experimental setup of Franson-type interference is based on the setup shown in Fig. 2A while two commercial unbalanced Mach-Zehnder interferometers (UMZIs) are placed before detection by SNSPDs. The unbalanced time between the two arms of the UMZI is 400 ps, which is much larger than the single-photon coherence time in the experiment to avoid single-photon interference. The phase shifter is on one arm of the UMZI and is tuned by applying a voltage. We fix the voltage of UMZI1 to be 1 and 2 V to construct two nonorthogonal bases and change the voltage of UMZI2 to obtain the two-photon interference fringes. The time bin for coincidence measurement is 50 ps and the coincidence counts are collected within the central 5 bins of the central coincidence peak. The pump condition, quantum light source, and filtering devices are the same as those in the JSI measurement.

Key generation

In the DO-QKD protocol, a high-dimensional encoding format is used to effectively exploit each single-photon event (*31*, *32*). It generates keys in a three-level sifting process (*39*). The continuous time of the two users is divided into time frames, time slots, and time bins. A time frame consists of $M = 2^D$ time slots, and a time slot contains I time bins. The time bin has a width of τ. Time frames are numbered sequentially. In addition, time slots in each frame and time bins in each slot are numbered sequentially and separately. In the process of key generation, Alice and Bob first select the time frames that contain only one single-photon event and discard other frames. Then, the frame number and bin number of each single-photon event are communicated through a classical channel. They pair the single-photon events that have the same frame number and bin number. Last, the raw keys are generated by the slot number.

The encoding parameters are optimized between users before the QKD starts (*39*). A higher encoding dimension or a larger time bin width may increase the raw key rate; however, it would result in a higher quantum bit error rate (QBER). The QBER influences the efficiency of the information reconciliation process. Hence, a trade-off is necessary between the raw key rate and QBER. In our DO-QKD scheme, the parameter optimization is carried out while the QBER is set to below an upper bound to obtain a relatively good reconciliation efficiency. See section S4 for more details.

Security analysis

In previous works, the security analysis of DO-QKD was discussed in detail (*31*–*33*). It is based on the treatment of single-photon events and the well-established proofs of Gaussian continuous-variable QKD (*44*, *45*). The time-frequency covariance matrix between the photons' arrival times of Alice and Bob is calculated. Then, the secure key capacity is calculated, which represents the number of secure keys that can be extracted from each coincidence count. It is denoted as

$$\Delta I = \beta I(\mathrm{A};\mathrm{B}) - \chi(\mathrm{A};\mathrm{E}) - \Delta_{\mathrm{FK}} \tag{1}$$

where β is the reconciliation efficiency, $I(\mathrm{A};\mathrm{B})$ is Shannon mutual information between Alice and Bob, $\chi(\mathrm{A};\mathrm{E})$ is Eve's Holevo information, and Δ_{FK} accounts for the penalty of the finite-size effect. In the process of bounding Eve's Holevo information, the excess noise factor ξ is estimated to quantify the disturbance from the eavesdropper, channel noise, and setup imperfections on the time-frequency covariance matrix. It represents an increase in the correlation time between entangled photon pairs, which can be denoted as

$$\xi = \frac{\sigma'^{2}_{\mathrm{cor}}}{\sigma^{2}_{\mathrm{cor}}} - 1 \tag{2}$$

where σ'_{cor} is the correlation time after transmission and σ_{cor} is an ideal noiseless result. We use the back-to-back correlation time in the experiment to approximate the ideal noiseless result. The Shannon information is calculated by estimating the correlation coefficient of the photons' arrival times between Alice and Bob.

When considering the finite-size effect, each stage of the QKD protocol has a probability of failing. The calculation of secure key capacity includes a subtraction

$$\Delta_{\mathrm{FK}} = \frac{1}{n} n_{\mathrm{ver}} + \frac{2}{n}\log_2\frac{1}{\varepsilon_{\mathrm{PA}}} + \left(2\log_2 M + 3\right)\sqrt{\frac{\log_2\left(\frac{2}{\bar{\varepsilon}}\right)}{n}} \tag{3}$$

where n is the number of coincidence counts devoted to key generation, n_{ver} is the information leakage in the verification step after error correction, $\varepsilon_{\mathrm{PA}}$ is the failure probability of privacy amplification, and $\bar{\varepsilon}$ is the failure probability of smooth min-entropy estimation. In addition, an uncertainty in estimating correlation time is considered in the finite size regime (*33*).

Supplementary Materials

This PDF file includes:

Sections S1 to S6
Figs. S1 to S13
Tables S1 to S4
References

REFERENCES AND NOTES

1. S. Wehner, D. Elkouss, R. Hanson, Quantum internet: A vision for the road ahead. *Science* **362**, eaam9288 (2018).
2. N. Gisin, G. Ribordy, W. Tittel, H. Zbinden, Quantum cryptography. *Rev. Mod. Phys.* **74**, 145–195 (2002).
3. S. Pirandola, U. L. Andersen, L. Banchi, M. Berta, D. Bunandar, R. Colbeck, D. Englund, T. Gehring, C. Lupo, C. Ottaviani, J. L. Pereira, M. Razavi, J. Shamsul Shaari, M. Tomamichel, V. C. Usenko, G. Vallone, P. Villoresi, P. Wallden, Advances in quantum cryptography. *Adv. Opt. Photonics* **12**, 1012–1236 (2020).
4. F. Xu, X. Ma, Q. Zhang, H.-K. Lo, J.-W. Pan, Secure quantum key distribution with realistic devices. *Rev. Mod. Phys.* **92**, 025002 (2020).
5. C. H. Bennett, G. Brassard, C. Crépeau, R. Jozsa, A. Peres, W. K. Wootters, Teleporting an unknown quantum state via dual classical and Einstein-Podolsky-Rosen channels. *Phys. Rev. Lett.* **70**, 1895–1899 (1993).
6. D. Bouwmeester, J.-W. Pan, K. Mattle, M. Eibl, H. Weinfurter, A. Zeilinger, Experimental quantum teleportation. *Nature* **390**, 575–579 (1997).
7. J. I. Cirac, A. K. Ekert, S. F. Huelga, C. Macchiavello, Distributed quantum computation over noisy channels. *Phys. Rev. A* **59**, 4249–4254 (1999).
8. V. Giovannetti, S. Lloyd, L. Maccone, Quantum-enhanced measurements: Beating the standard quantum limit. *Science* **306**, 1330–1336 (2004).
9. X. Guo, C. R. Breum, J. Borregaard, S. Izumi, M. V. Larsen, T. Gehring, M. Christandl, J. S. Neergaard-Nielsen, U. L. Andersen, Distributed quantum sensing in a continuous-variable entangled network. *Nat. Phys.* **16**, 281–284 (2019).
10. A. Acín, N. Brunner, N. Gisin, S. Massar, S. Pironio, V. Scarani, Device-independent security of quantum cryptography against collective attacks. *Phys. Rev. Lett.* **98**, 230501 (2007).

11. S. Pironio, A. Acín, N. Brunner, N. Gisin, S. Massar, V. Scarani, Device-independent quantum key distribution secure against collective attacks. *New J. Phys.* **11**, 045021 (2009).
12. I. Herbauts, B. Blauensteiner, A. Poppe, T. Jennewein, H. Hübel, Demonstration of active routing of entanglement in a multi-user network. *Opt. Express* **21**, 29013–29024 (2013).
13. A. Ciurana, V. Martin, J. Martinez-Mateo, B. Schrenk, M. Peev, A. Poppe, Entanglement distribution in optical networks. *IEEE J. Sel. Top. Quantum Electron.* **21**, 37–48 (2015).
14. X. Y. Chang, D. L. Deng, X. X. Yuan, P. Y. Hou, Y. Y. Huang, L. M. Duan, Experimental realization of an entanglement access network and secure multi-party computation. *Sci. Rep.* **6**, 29453 (2016).
15. X. Liu, X. Yao, R. Xue, H. Wang, H. Li, Z. Wang, L. You, X. Feng, F. Liu, K. Cui, Y. Huang, W. Zhang, An entanglement-based quantum network based on symmetric dispersive optics quantum key distribution. *APL Photon.* **5**, 076104 (2020).
16. S. Wengerowsky, S. K. Joshi, F. Steinlechner, H. Hübel, R. Ursin, An entanglement-based wavelength-multiplexed quantum communication network. *Nature* **564**, 225–228 (2018).
17. S. K. Joshi, D. Aktas, S. Wengerowsky, M. Lončarić, S. P. Neumann, B. Liu, T. Scheidl, G. C. Lorenzo, Ž. Samec, L. Kling, A. Qiu, M. Razavi, M. Stipčević, J. G. Rarity, R. Ursin, A trusted node–free eight-user metropolitan quantum communication network. *Sci. Adv.* **6**, DOI: 10.1126/sciadv.aba0959 (2020).
18. X. Liu, J. Liu, R. Xue, H. Wang, H. Li, X. Feng, F. Liu, K. Cui, Z. Wang, L. You, Y. Huang, W. Zhang, 40-user fully connected entanglement-based quantum key distribution network without trusted node. *PhotoniX* **3**, 2 (2022).
19. M. Alshowkan, B. P. Williams, P. G. Evans, N. S. V. Rao, E. M. Simmerman, H.-H. Lu, N. B. Lingaraju, A. M. Weiner, C. E. Marvinney, Y.-Y. Pai, B. J. Lawrie, N. A. Peters, J. M. Lukens, Reconfigurable quantum local area network over deployed fiber. *PRX Quantum* **2**, 040304 (2021).
20. F. Appas, F. Baboux, M. I. Amanti, A. Lemaître, F. Boitier, E. Diamanti, S. Ducci, Flexible entanglement-distribution network with an AlGaAs chip for secure communications. *npj Quantum Inf.* **7**, 118 (2021).
21. N. B. Lingaraju, H.-H. Lu, S. Seshadri, D. E. Leaird, A. M. Weiner, J. M. Lukens, Adaptive bandwidth management for entanglement distribution in quantum networks. *Optica* **8**, 329–332 (2021).
22. R. Wang, O. Alia, M. J. Clark, S. Bahrani, S. K. Joshi, D. Aktas, G. T. Kanellos, M. Peranić, M. Lončarić, M. Stipčević, J. Rarity, R. Nejabati, D. Simeonidou, A dynamic multi-protocol entanglement distribution quantum network, in *2022 Optical Fiber Communications Conference and Exhibition (OFC)* (IEEE, 2022), pp. 1-3.
23. R. Wang, M. J. Clark, S. K. Joshi, S. Bahrani, O. Alia, M. Peranić, M. Lončarić, M. Stipčević, J. Rarity, R. Nejabati, D. Simeonidou, Optimum switching scenario analysis in a dynamic entanglement network, in *2023 Optical Fiber Communications Conference and Exhibition (OFC)* (IEEE, 2023).
24. G. P. Agrawal, Four-wave mixing, in *Nonlinear Fiber Optics* (Academic Press, ed. 6, 2019), chap. 10, pp. 401–462.
25. Q. Lin, F. Yaman, G. P. Agrawal, Photon-pair generation in optical fibers through four-wave mixing: Role of Raman scattering and pump polarization. *Phys. Rev. A* **75**, 023803 (2007).
26. K. Garay-Palmett, H. J. McGuinness, O. Cohen, J. S. Lundeen, R. Rangel-Rojo, A. B. U'Ren, M. G. Raymer, C. J. McKinstrie, S. Radic, I. A. Walmsley, Photon pair-state preparation with tailored spectral properties by spontaneous four-wave mixing in photonic-crystal fiber. *Opt. Express* **15**, 14870–14886 (2007).
27. B. Fang, O. Cohen, J. B. Moreno, V. O. Lorenz, State engineering of photon pairs produced through dual-pump spontaneous four-wave mixing. *Opt. Express* **21**, 2707–2717 (2013).
28. L. Yu, C. Yuan, R. Qi, Y. Huang, W. Zhang, Hybrid waveguide scheme for silicon-based quantum photonic circuits with quantum light sources. *Photon. Res.* **8**, 235–245 (2020).
29. J.-P. Wu, Y.-R. Fan, H. Zeng, H. Li, Y. Wang, G.-W. Deng, L.-X. You, Z. Wang, H.-Z. Song, G.-C. Guo, Q. Zhou, Multi-wavelength Quantum Light Source with Dual Pumps, in *2023 Asia Communications and Photonics Conference/2023 International Photonics and Optoelectronics Meetings (ACP/POEM)* (IEEE, 2023), pp. 1–3.
30. J. D. Franson, Nonlocal cancellation of dispersion. *Phys. Rev. A* **45**, 3126–3132 (1992).
31. J. Mower, Z. Zhang, P. Desjardins, C. Lee, J. H. Shapiro, D. Englund, High-dimensional quantum key distribution using dispersive optics. *Phys. Rev. A* **87**, 062322 (2013).
32. C. Lee, Z. Zhang, G. R. Steinbrecher, H. Zhou, J. Mower, T. Zhong, L. Wang, X. Hu, R. D. Horansky, V. B. Verma, A. E. Lita, R. P. Mirin, F. Marsili, M. D. Shaw, S. W. Nam, G. W. Wornell, F. N. C. Wong, J. H. Shapiro, D. Englund, Entanglement-based quantum communication secured by nonlocal dispersion cancellation. *Phys. Rev. A* **90**, 062331 (2014).
33. C. Lee, J. Mower, Z. Zhang, J. H. Shapiro, D. Englund, Finite-key analysis of high-dimensional time–energy entanglement-based quantum key distribution. *Quantum Inf. Process.* **14**, 1005–1015 (2015).
34. S. Azzini, D. Grassani, M. Galli, L. C. Andreani, M. Sorel, M. J. Strain, L. G. Helt, J. E. Sipe, M. Liscidini, D. Bajoni, From classical four-wave mixing to parametric fluorescence in silicon microring resonators. *Opt. Lett.* **37**, 3807–3809 (2012).
35. Q. Li, M. Davanço, K. Srinivasan, Efficient and low-noise single-photon-level frequency conversion interfaces using silicon nanophotonics. *Nat. Photon.* **10**, 406–414 (2016).
36. J. D. Franson, Bell inequality for position and time. *Phys. Rev. Lett.* **62**, 2205–2208 (1989).
37. J. F. Clauser, M. A. Horne, A. Shimony, R. A. Holt, Proposed experiment to test local hidden-variable theories. *Phys. Rev. Lett.* **23**, 880–884 (1969).
38. I. Marcikic, H. de Riedmatten, W. Tittel, H. Zbinden, M. Legre, N. Gisin, Distribution of time-bin entangled qubits over 50 km of optical fiber. *Phys. Rev. Lett.* **93**, 180502 (2004).
39. X. Liu, X. Yao, H. Wang, H. Li, Z. Wang, L. You, Y. Huang, W. Zhang, Energy-time entanglement-based dispersive optics quantum key distribution over optical fibers of 20 km. *Appl. Phys. Lett.* **114**, 141104 (2019).
40. J. M. Lukens, P. Lougovski, Frequency-encoded photonic qubits for scalable quantum information processing. *Optica* **4**, 8–16 (2017).
41. P. Imany, N. B. Lingaraju, M. S. Alshaykh, D. E. Leaird, A. M. Weiner, Probing quantum walks through coherent control of high-dimensionally entangled photons. *Sci. Adv.* **6**, eaba8066 (2020).
42. U. A. Javid, R. Lopez-Rios, J. Ling, A. Graf, J. Staffa, Q. Lin, Chip-scale simulations in a quantum-correlated synthetic space. *Nat.Photon.* **17**, 883–890 (2023).
43. R. Raussendorf, H. J. Briegel, A one-way quantum computer. *Phys. Rev. Lett.* **86**, 5188–5191 (2001).
44. A. Serafini, F. Illuminati, S. D. Siena, Symplectic invariants, entropic measures and correlations of Gaussian states. *J. Phys. B: At. Mol. Opt. Phys.* **37**, L21–L28 (2004).
45. R. García-Patrón, N. J. Cerf, Unconditional optimality of Gaussian attacks against continuous-variable quantum key distribution. *Phys. Rev. Lett.* **97**, 190503 (2006).
46. Q. Zhou, W. Zhang, J.-r. Cheng, Y.-d. Huang, J.-d. Peng, Properties of optical fiber based synchronous heralded single photon sources at 1.5 μm. *Phys. Lett. A* **375**, 2274–2277 (2011).
47. S. Krapick, H. Herrmann, V. Quiring, B. Brecht, H. Suche, C. Silberhorn, An efficient integrated two-color source for heralded single photons. *New J. Phys.* **15**, 033010 (2013).
48. J. Liu, Z. Lin, D. Liu, X. Feng, F. Liu, K. Cui, Y. Huang, W. Zhang, High-dimensional quantum key distribution using energy-time entanglement over 242 km partially deployed fiber. *Quantum Sci. Technol.* **9**, 015003 (2024).
49. E. O. Kiktenko, A. S. Trushechkin, C. C. W. Lim, Y. V. Kurochkin, A. K. Fedorov, Symmetric blind information reconciliation for quantum key distribution. *Phys. Rev. Applied* **8**, 044017 (2017).
50. H. Zhou, L. Wang, G. Wornell, Layered Schemes for Large-Alphabet Secret Key Distribution, in *2013 Information Theory and Applications Workshop (ITA)* (IEEE, 2013), pp. 1–10.
51. J.-Y. Liu, X. Liu, W. Zhang, Y.-D. Huang, Impact of fiber dispersion on the performance of entanglement-based dispersive optics quantum key distribution. *J. Electron. Sci. Technol.* **19**, 297–307 (2021).

Acknowledgments

Funding: This work was supported by the National Natural Science Foundation of China (92365210, W.Z.), the National Key R&D Program of China (2023YFB2806700, Y.H.), the Tsinghua Initiative Scientific Research Program (W.Z.), and the project of Tsinghua University-Zhuhai Huafa Industrial Share Company Joint Institute for Architecture Optoelectronic Technologies (JIAOT, Y.H.). **Author contributions:** Conceptualization: J.L. and W.Z. Funding acquisition: X.F., F.L., K.C., W.Z., and Y.H. Investigation: J.L., D.L., Z.L., and W.Z. Methodology: J.L., D.L., and W.Z. Project administration: W.Z. and Y.H. Resources: Z.J., H.L., and L.Y. Supervision: X.F., F.L., K.C., W.Z., and Y.H. Visualization: J.L. Writing—original draft: J.L. and W.Z. Writing—review and editing: J.L., H.L., and W.Z. **Competing interests:** The authors declare that they have no competing interests. **Data and materials availability:** All data needed to evaluate the conclusions in the paper are present in the paper and/or the Supplementary Materials.

Submitted 1 March 2024
Accepted 6 November 2024
Published 13 December 2024
10.1126/sciadv.ado9822